Polymer composite material characterisation using a laser/air-transducer system

W.M.D. Wright [a,*], D.A. Hutchins [a], A. Gachagan [b], G. Hayward [b]

[a] *Department of Engineering, University of Warwick, Coventry CV4 7AL, UK*
[b] *Department of Electrical and Electronic Engineering, University of Strathclyde, Glasgow G1 1XW, UK*

Abstract

A wide bandwidth 1–3 connectivity piezocomposite air transducer has been used to detect laser-generated ultrasound in a variety of composite materials. Through thickness waveforms in various carbon fibre reinforced polymer (CFRP) composite plates will be presented, as well as a selection of Lamb waves. Signals were also obtained in samples of pultruded glass fibre reinforced composite of different thickness. Using the laser/air-transducer system, images were obtained of machined defects and delaminations by conventional C-scanning methods, and tomographic reconstruction techniques.

Keywords: Air-coupled transducer; Non-contact ultrasound; Fibre-reinforced composites; C-scan imaging; Lamb wave tomography

1. Introduction

Composite materials [1–3] have numerous applications in engineering, as their structure and properties may give many advantages over conventional materials. In particular, these materials are being used in the automotive and aerospace industries, where weight must be saved without sacrificing strength. A composite material typically consists of a base matrix that has been modified by the addition of a strengthening material, usually in the form of particles, chopped strands or whiskers, or continuous fibres. As with any other engineering material or application, components made from a composite material must be tested for defects to ensure their reliability in service. There are many different non-destructive testing techniques which may be applied, and the use of ultrasonics is well documented [4–6]. Traditional contact testing methods have been used to test for defects, but as always, there are applications and situations where contact with the test specimen is either undesirable or impossible. Some forms of composite are absorbent to fluids, and so immersion techniques and conventional wet couplants cannot be used. In other cases, rapid inspection of large structures such as aircraft wing panels [7] is required, and any form of contact will significantly increase the inspection times.

There are several non-contact techniques cited in the literature, but few are suitable or readily applied to composite materials. The use of electromagnetic acoustic transducers (EMATs) [8] and capacitance devices [9] is restricted to electrically conductive materials. Laser based systems [10] encounter practical problems when testing composite materials, in that composites tend to have rough surfaces and poor optical reflectivity. Hence, most interferometers and other laser based detectors are either unsuitable or too expensive and delicate. As sources of ultrasound, pulsed lasers have been successfully used in many situations [11–13], and so the main problem seems to be the lack of a suitable detector. Air-coupled transducers show promise for this application, and a variety of different designs are available. The devices may be divided into two distinct groups, electrostatic or capacitance transducers [14–20] which use a thin metallised polymer membrane and a contoured conducting backplate, and piezoelectric transducers which are either piezopolymers [21,22], piezoceramics with a suitable matching layer [23], or piezocomposites [24–27]. The work to be described here will demonstrate that piezocomposite air-coupled transducers are well

* Corresponding author.
e-mail: es770@eng.warwick.ac.uk; Fax: +44-1203-418-922.

suited to act as detectors of laser-generated ultrasound in an entirely non-contact detection system, and follows on from earlier work where a hybrid laser source/air-coupled detector was shown to produce good waveforms in metals [28]. This work has been extended to cover composite materials, using wider bandwidth detectors, where it will be shown that non-contact imaging is possible.

2. The composite materials

Two types of composite material were studied. The first of these, made by Fibreforce Composites Ltd., was a selection of pultruded composites [1] and are so named after their method of manufacture. Fibre bundles or rovings of unidirectional 10 μm diameter E-glass fibres (local volume fraction 62%), and continuous filament mats of E-glass fibres (local volume fraction 28%) are pulled through a bath of isophthalic polyester resin containing 10–15% by volume of calcium carbonate, and passed through a series of rollers and curing equipment in a continuous process. The weights of mat and roving used were approximately equal, but the exact amounts were unknown as the manufacturer considered this information proprietary. The resulting material has a fairly random structure as limited control over the fibre orientation is available. Although not particularly anisotropic, in practice this material is extremely scattering and attenuating to ultrasound, and is in most respects a 'worst case'. The second group of materials were carbon fibre reinforced polymer (CFRP) composites [2,3], and were manufactured by arranging layers of carbon fibres (Enka Tenax HTA in 12K tows) pre-impregnated with epoxy resin (ICI 7716H) in the desired orientations, and then compression moulding them in a heated press at 120°C. This allowed the composite structure to be precisely controlled, and so composites can be classified as unidirectional (all fibres running parallel to the principle fibre axis), cross-ply (fibre layers alternately at 0° and 90° to the principal fibre axis), and quasi-isotropic (fibre layers alternately at 0°, −45°, +45° and 90° to the principle fibre axis). The nominal fibre content was 60% by volume which is typical of this type of composite.

3. The non-contact system

The components of the laser/air-transducer system are shown schematically in Fig. 1. Ultrasonic waves were generated in a composite sample by a CO_2 TEA laser, delivering 100 ns pulses at 10.6 μm with a total energy of approximately 8 J. These waves were detected using a wideband piezocomposite transducer and an air gap of 15 mm between the sample and detector was main-
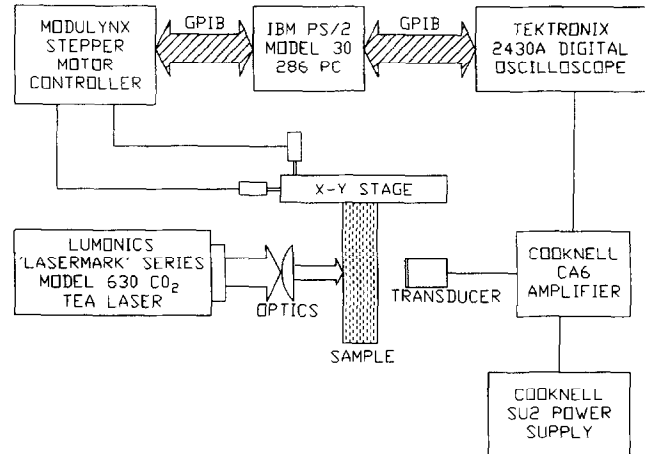

Fig. 1. Schematic diagram of the laser/air-transducer system.

tained throughout the experiments. Signals were amplified using a Cooknell CA6 charge amplifier, captured using a Tektronix 2430A digital oscilloscope, and transferred to an IBM PS/2 Model 30 286 PC for storage and analysis via an IEEE-488/GPIB interface. The computer was also used to move the composite sample using a Modulynx stepper motor controller, and an X–Y stage for C-scan images or a linear/rotary stage combination for tomographic imaging.

4. Piezocomposite receiver design

A 1–3 connectivity composite transducer comprises an array of piezoceramic pillars embedded within a passive (usually polymer) filler material. The normal structure is shown in Fig. 2, where the piezoceramic pillars are designed to be tall and thin to promote uniform vibration in the height of thickness direction.
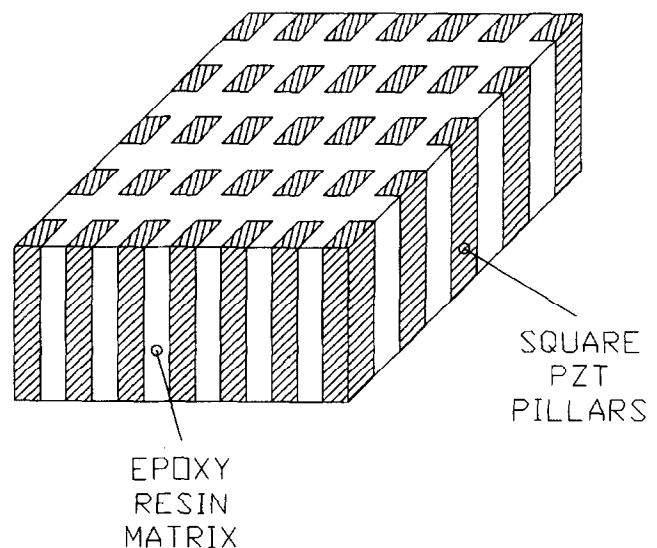

Fig. 2. A 1–3 connectivity PZT/epoxy composite element.

The properties of such a transducer depend strongly on the ceramic volume fraction, pillar shape and distribution, and the characteristics of the filler material. In theory, composite transducer behaviour may be configured and optimised for a specific application by the relatively straightforward adjustment of these parameters. However the inter relationships between volume fraction and operational parameters such as mechanical and electrical impedance, electrical interfacing and transmission sensitivity often necessitate a compromise and some form of computer modelling is required for optimisation of composite performance. Both linear systems [26,29] and finite element [27,29,30] modelling approaches have been successfully applied for prediction of 1–3 composite transducers behaviour. The former is a uni-dimensional technique that assumes the composite behaves as an effective homogeneous medium. The approximation is valid if the composite possesses a sufficiently fine spatial scale such that all lateral and inter-pillar resonances are shifted away from the desired thickness mode. Under certain conditions, this assumption is no longer valid and hence, a more computationally intensive finite element approach would be required for the comprehensive evaluation of composite behaviour. Hence, understanding and optimisation of piezo-composite behaviour under such conditions is extremely complex, especially at the lower volume fractions required for reception applications. Indeed, comprehensive design guidelines are available to quantify the maximum allowable pillar width to height ratio for a specific volume fraction [30].

The laser generation/piezoelectric detection hybrid system comprises essentially a wideband point source coupled with an inherently narrowband receiver of finite aperture. Initial experimentation using prototype air-coupled transducers was described in earlier work [28], where the remote acoustic detection of laser-generated longitudinal and shear bulk modes, Rayleigh waves and various types of Lamb waves was demonstrated. However, the resonant nature of the detectors employed in this work required the application of deconvolution techniques to enhance system resolution capabilities.

In order to progress from this earlier work, it was necessary to create a reception device of sufficient sensitivity and bandwidth to complement the high resolution afforded by laser generation. Here, a novel approach to the design of 1–3 connectivity composite transducers has been adopted, where the first inter-pillar resonance can actually be used to extend bandwidth, at the expense of coupling coefficient and surface uniformity. Finite element analysis was used to predict the receive bandwidth, defined as the −6 dB bandwidth expressed as a percentage of the transducer centre frequency, for the transducer, as the ceramic pillar width to height (aspect) ratio was varied. In this analysis, the ceramic pillar width and inter-pillar spacing have been kept constant
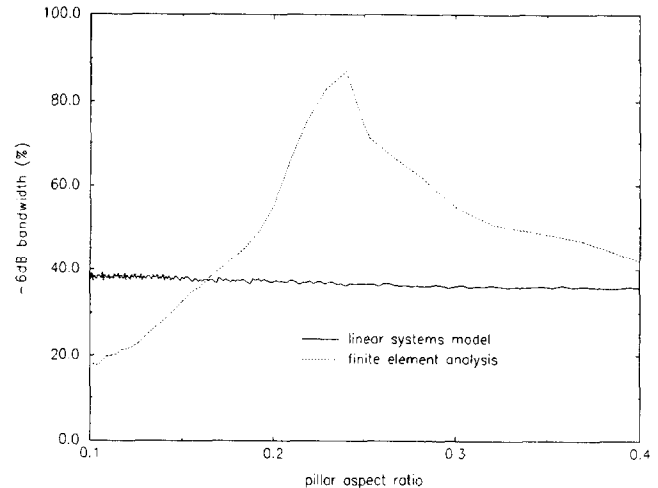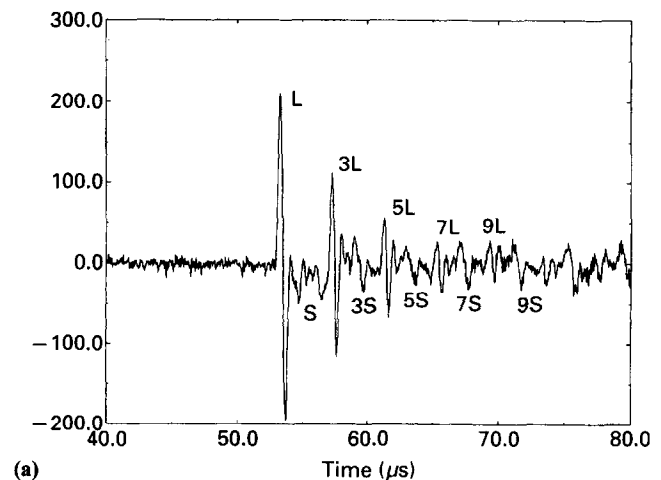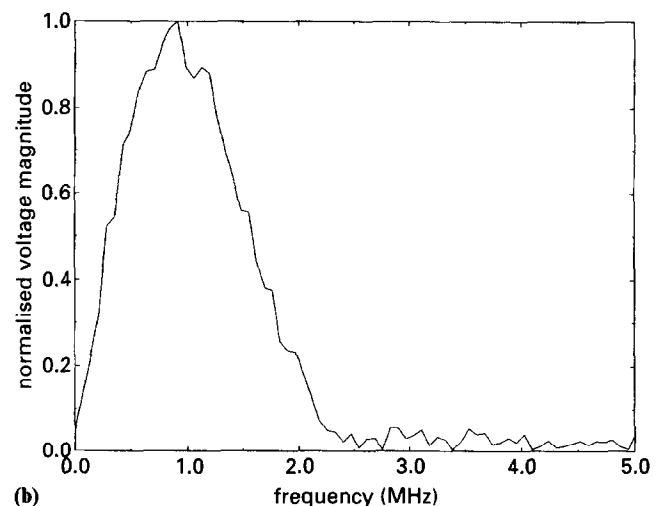

Fig. 3. Predicted bandwidth improvement due to coupling between the first lateral and fundamental resonances in a 1–3 composite transducer.

(a)

(b)

Fig. 4. (a) Air-coupled detection of laser-generated ultrasound in 12.8 mm aluminium. (b) Frequency spectrum of a single longitudinal reflection (L) from (a).

and the transducer thickness varied between 0.6 mm and 2.5 mm, resulting in a spread of aspect ratios from 0.4 to 0.1, respectively. The results from this analysis are presented in Fig. 3, where it can be observed that the finite element analysis has predicted a large gain in bandwidth for an aspect ratio of 0.24. The linear systems model is included to estimate the transducer bandwidth when the presence of the lateral mode is effectively removed from the analysis.

To evaluate the predicted enhancement in bandwidth for a 'laterally-coupled' composite receiver, laser-generated ultrasound in 12.8 mm thick aluminium has been

detected. The transducer (aspect ratio of 0.24) was constructed from a 15 mm PZT5A ceramic disc and utilised Ciba-Geigy CY1300/HY1301 hard setting epoxy as the filler material. The received signal, in single shot mode, is shown in Fig. 4(a), from which it can be observed that the wide bandwidth allows both discrete multiple longitudinal reflections (L, 3L, etc.) to be seen, as well as a shear arrival (S) and subsequent mode conversions (3S, 5S, etc.). To illustrate the operational bandwidth of this device, the frequency spectrum of a single through air longitudinal reflection is shown in Fig. 4(b). This constitutes a −6 dB system bandwidth
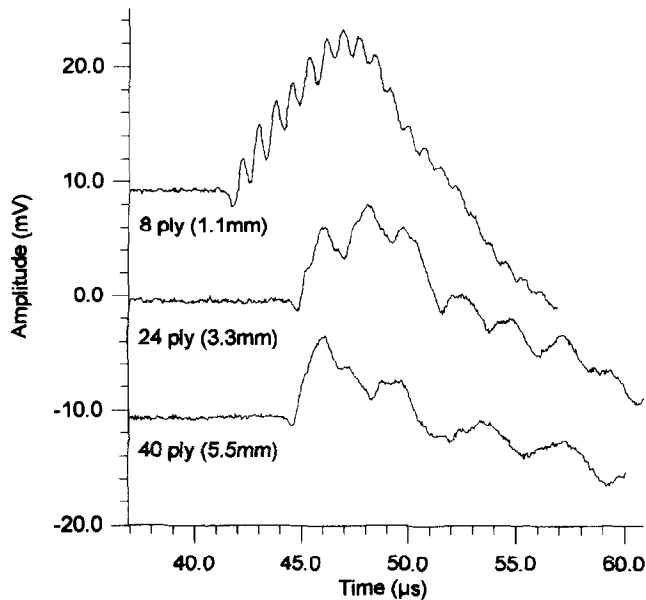
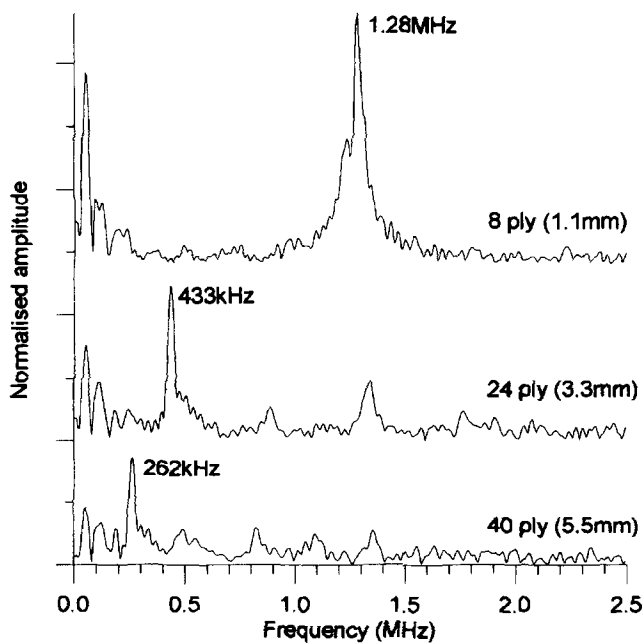

Fig. 5. Through thickness waveforms in CFRP.
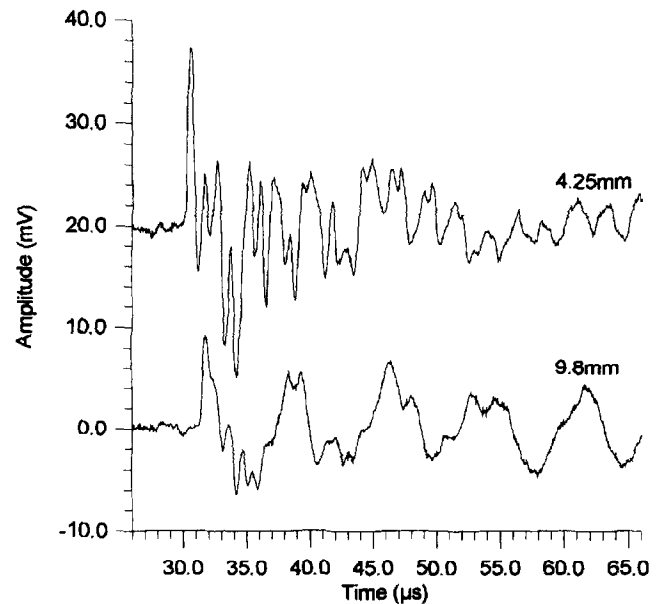

Fig. 7. Through thickness waveforms in pultruded composite.

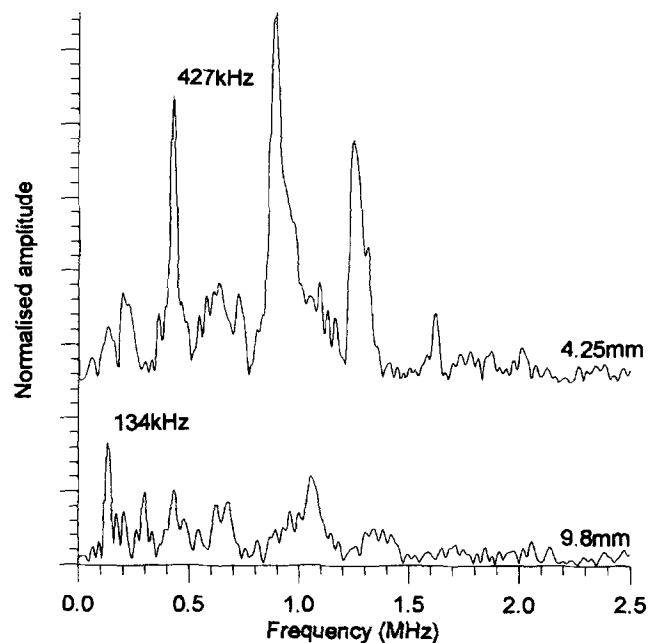Fig. 6. Frequency spectra of waveforms in Fig. 5.

Fig. 8. Frequency spectra of waveforms in Fig. 7.

of approximately 150%, with respect to the 950 kHz centre frequency.

5. Through thickness waveforms and C-scan imaging

Many waveforms were taken in a variety of composite samples, and so only a fraction will be presented here. Fig. 5 shows three through thickness waveforms detected in (a) an 8 ply (1.1 mm thick), (b) a 24 ply (3.3 mm thick), and (c) a 40 ply (5.5 mm thick) quasi-isotropic CFRP composite. It can be seen that the wave sets up a resonant frequency which is determined by the thickness of the plate, as can be seen in Fig. 6 where the fast Fourier transforms (FFTs) of the differentiated signals in Fig. 5(a–c) are presented. In conjunction with the known thickness d of each sample, this frequency f may be used to evaluate the longitudinal acoustic velocity c_L

by:

$$c_L = 2fd. \tag{1}$$

The measured frequencies for the 8 ply, 24 ply and 40 ply plates were 1.282 MHz, 433 kHz and 262 kHz respectively (± 6.1 kHz), giving values for c_L of 2820 ms^{-1}, 2860 ms^{-1} and 2887 ms^{-1} respectively (± 13 ms^{-1}). Similar waveforms were obtained in samples of unidirectional and cross-ply composite of the same thickness, as the bulk through thickness velocities are virtually unaffected by the different fibre orientations. Signals were also obtained in samples of pultruded glass fibre reinforced composite with different matrix polymers. Examples are presented in Fig. 7 for (a) 4 mm thick and (b) 9.8 mm thick specimens respectively, and the corresponding frequency spectra are shown in Fig. 8. The relevant resonant peaks were at 427 kHz and 134 kHz respectively (± 6.1 kHz), with other resonant peaks also present. These frequencies gave velocities of 3418 ms^{-1} and 2632 ms^{-1} (± 13 ms^{-1}) for the thin and thick samples, respectively. These velocities were also measured using conventional piezoelectric probes and found to be correct, and so the inequality may be attributed to the different matrix materials.

Using the laser/air-transducer system, and mounting the sample on a computer controlled X-Y stage, it was possible to produce images of a variety of defects using through thickness waveforms. By storing the digitised waveform at each point in the scan, it enabled customised software to apply a variety of data processing techniques in both the time and frequency domain, and thus resolve the defect. In each of the following images, the approximate size, shape and location of the defect is shown by a dashed line.
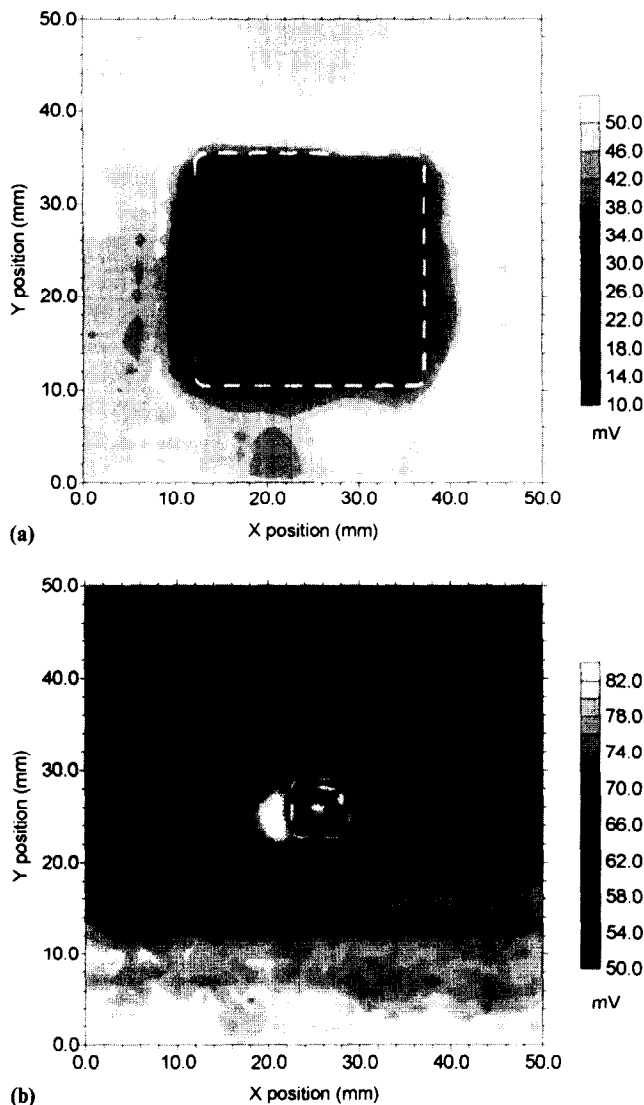
Fig. 9 shows (a) 25 mm and (b) 6 mm square

Fig. 9. C-scan image of (a) a 25 mm square and (b) a 6 mm square Teflon delamination in a 16 ply unidirectional CFRP plate.
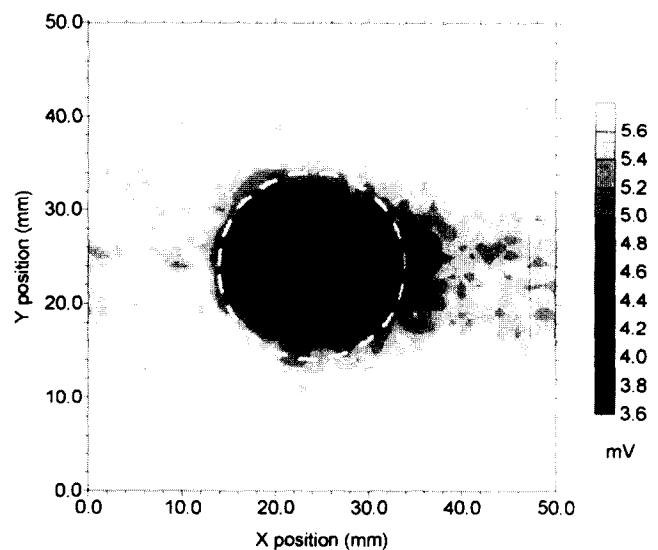

Fig. 10. C-scan image of a 10 mm flat bottomed hole in a 32 ply cross-ply CFRP plate.

delaminations in a 16 ply (2.2 mm) thick unidirectional CFRP composite, produced by replacing the centre 8 plies with 8 layers of Teflon tape during the manufacture of the plate. The size of each defect may be resolved with some accuracy, but the shape of the 6 mm square defect has been distorted due to the size of the source and receiver. Fig. 10 shows the image obtained by scanning a 10 mm diameter flat bottomed hole machined into a 32 ply (4.4 mm) cross-ply CFRP plate to approximately half the plate thickness. These images were obtained by simply measuring the signal amplitude in a specified time window. Fig. 11 shows images of another 10 mm diameter flat bottomed defect, this time machined to a depth of 1 mm into a 9.8 m thick sample of pultruded composite. Fig. 11(a) was obtained using the signal amplitude as before, and Fig. 11(b) was obtained

by measuring the shift in time of the first arrival. The hole may also be seen in the frequency domain, using the amplitude of a frequency window in Fig. 11(c), and the shift in frequency of a resonant peak in Fig. 11(d). The defect can be resolved using both techniques, despite being almost obscured by a horizontal feature caused by a resin rich area of composite.

6. Lamb waves and tomographic imaging

Lamb waves [31] were also obtained in thin sheets of composite, and again, only a selection of waveforms will be displayed here. Fig. 12 shows a range of Lamb wave signals taken in an 8 ply unidirectional CFRP composite plate, with the transducer at various angles
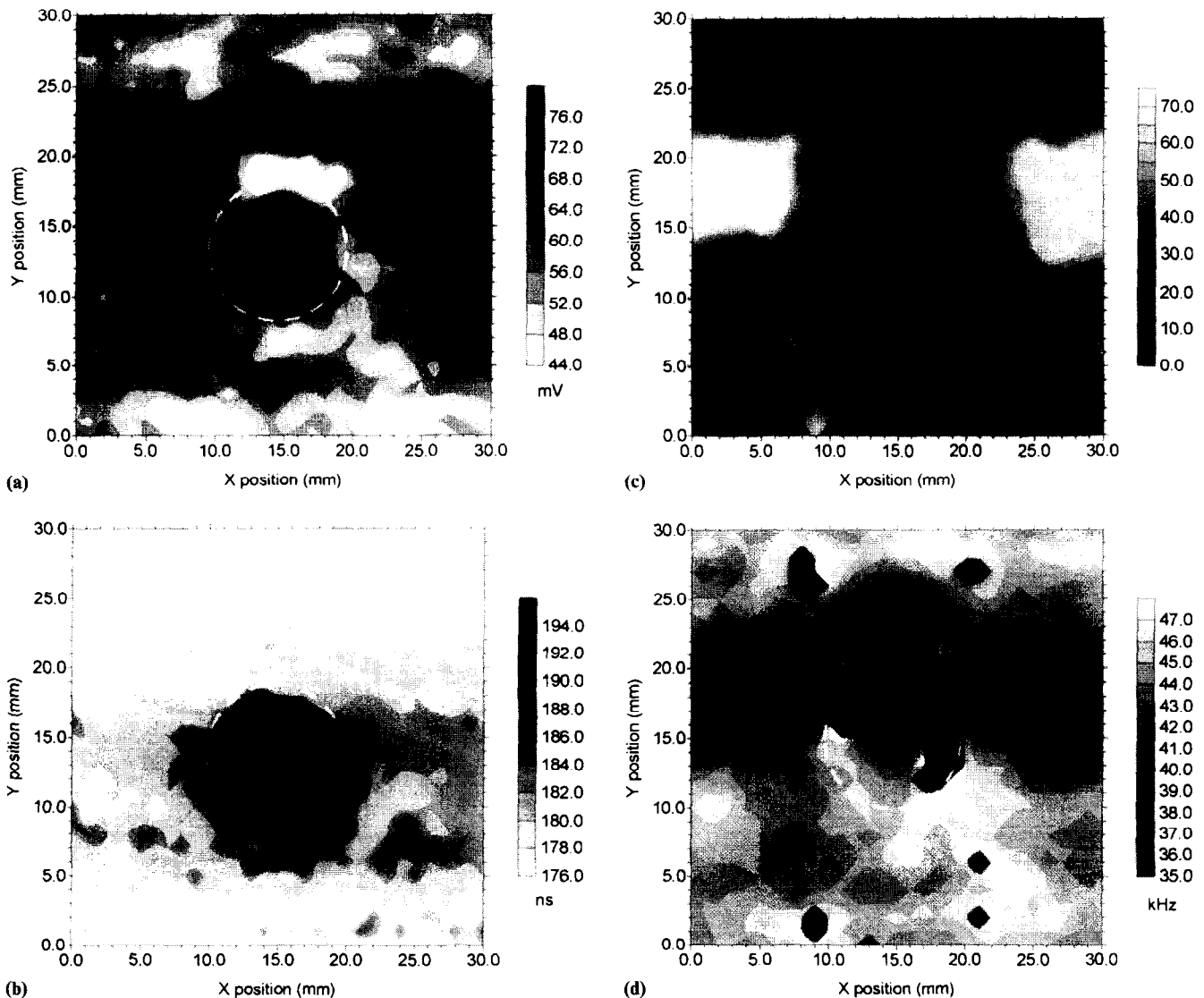

Fig. 11. C-scan images of a 10 mm diameter by 1 mm deep flat bottomed hole in a 9.8 mm sample of pultruded composite, formed by (a) amplitude of time domain waveform, (b) shift in time of flight, (c) amplitude in frequency spectrum (arbitrary grey scale), and (d) shift of peak in the frequency spectrum.

with respect to the surface of the plate, and the Lamb waves propagating parallel to the principle fibre axis over a distance of 50 mm. Lamb waves radiate or 'leak' into air at different angles depending on their frequency, and this can clearly be seen as the frequency content decreases as the angle increases. Fig. 13 shows the same scenario, but with the Lamb waves propagating perpendicular to the principle fibre axis. Note the markedly
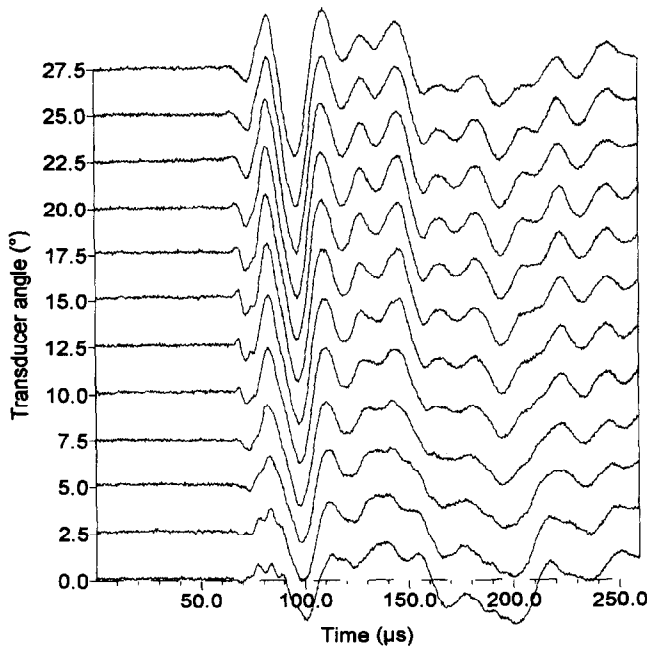
different waveform shapes for the same angle, due to the presence of different modes in the anisotropic material. Lamb waves were also obtained in the 4 mm thick samples of pultruded composite, with examples being shown in Fig. 14 travelling (a) parallel and (b) perpendicular to the direction of pultrusion, with the transducer at an angle of 2.5° to the sample. This material does not appear to possess such a high degree of anisotropy.

Lamb waves may also be used to image defects using tomographic reconstruction techniques [32–34]. With the laser source and air-transducer a fixed distance apart, Lamb waves may be propagated across the defect, and by moving the sample a small distance d perpendicular to the propagation direction and taking another waveform, a view or 'projection' through the defect may be

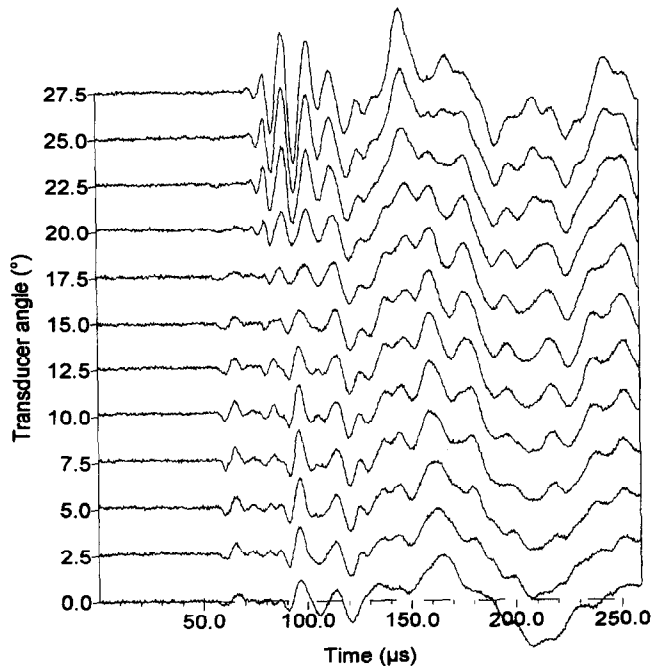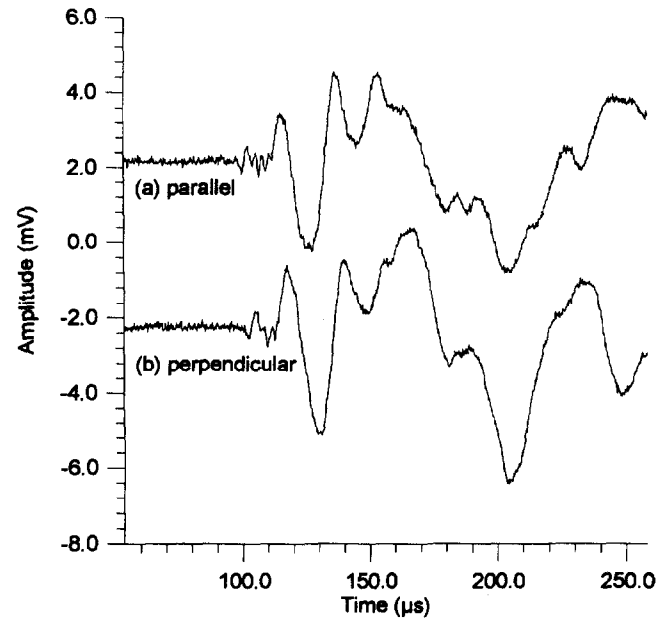Fig. 12. Lamb waves in an 8 ply unidirectional CFRP plate, travelling parallel to the principle fibre axis.

Fig. 14. Lamb waves in 4 mm pultruded composite, travelling (a) parallel and (b) perpendicular to the direction of pultrusion.

Fig. 13. Lamb waves in an 8 ply unidirectional CFRP plate, travelling perpendicular to the principle fibre axis.
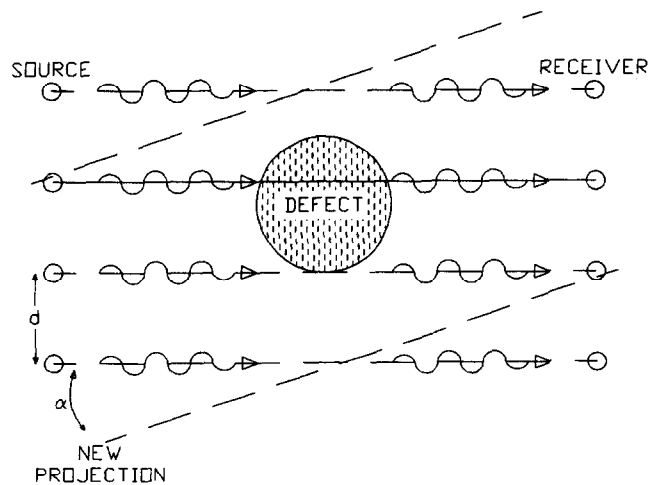

Fig. 15. Schematic diagram of a tomographic scan.

built up, each parallel waveform being known as a 'ray'. By rotating the sample through an angle α and repeating the process, a series of different projections can be built up, as shown schematically in Fig. 15. By using a filtered back projection algorithm [33,34], this series of projections may be reconstructed to produce an image of the defect, expressed as change in slowness (the inverse of velocity) or amplitude.

Fig. 16 shows a selection of images produced using this technique. The samples were rotated through 180° in 5° steps, giving 37 projections, and moved through 50 mm in 1 mm steps, producing 51 rays per projection. Fig. 16(a) shows the image produced for a 5 mm diameter hole drilled through a 1 mm thick sheet of polymethylmethacrylate (perspex), and Fig. 16(b) the image for the 10 mm diameter flat bottomed hole machined in the 32 ply cross-ply CFRP which was C-scanned earlier.
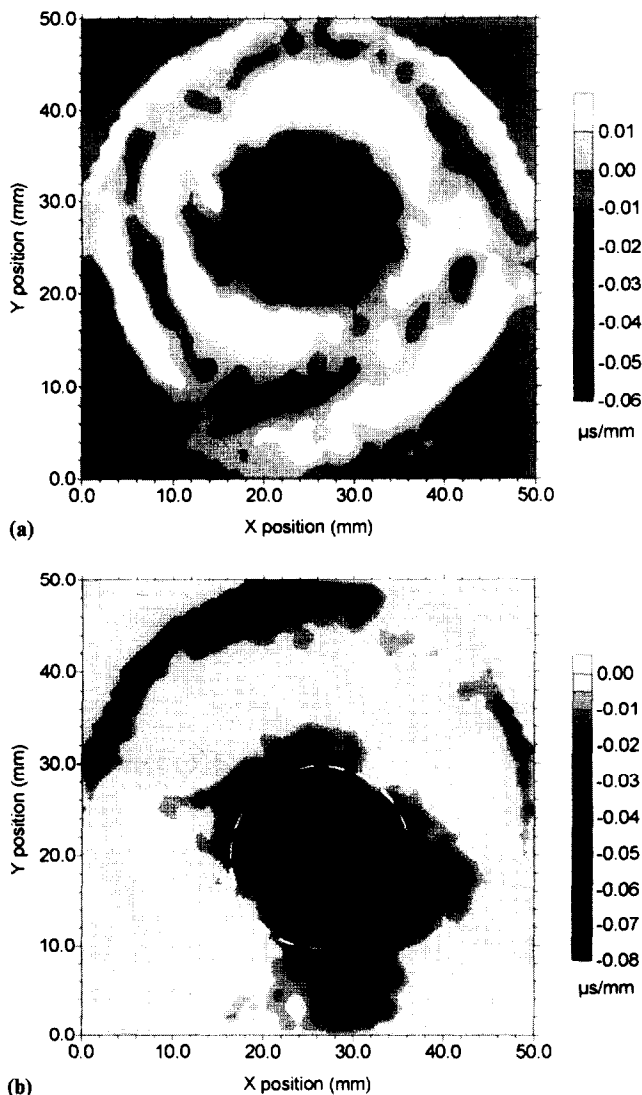

(a)

(b)

Fig. 16. Lamb wave tomography image of (a) a 5 mm diameter hole through a 1 mm PMMA sheet and (b) of the 10 mm diameter flat bottomed hole in a 32 ply cross-ply CFRP plate.

Both images were obtained by using the cross correlated time of flight shift of the low frequency a_0 mode, and the defects are clearly resolved by this technique.

7. Conclusions

A novel method for bandwidth extension of 1–3 connectivity PZT/epoxy composite transducers was employed in the detection of laser-generated ultrasound in composite materials. Here the composite spatial scale was configured such that interference between the thickness resonance and the first inter-pillar resonance resulted in an extremely wideband response. The hybrid laser/air-transducer system was used to evaluate both pultruded glass fibre reinforced composites, and carbon fibre reinforced polymer (CFRP) composite samples. Through thickness longitudinal waves were used to determine the acoustic velocity (and thus the elastic properties) of each material, as well as to produce images of both delaminations and machined defects by conventional C-scanning techniques. Lamb waves were also used to image these defects using a filtered back projection algorithm to reconstruct tomographic images. The non-contact ultrasonic inspection system described in this work shows promise in the rapid inspection of composites and other engineering materials.

References

[1] R.W. Meyer, Handbook of Pultrusion Technology (Chapman and Hall, New York, 1985).
[2] D. Hull, An Introduction to Composite Materials (Cambridge University Press, Cambridge, 1981).
[3] P.K. Mallick and S. Newman (Eds.), Composite Materials Technology: Process and Properties (Hanser, Munich, 1992).
[4] R.A. Blake, in: Delaware Composites Design Encyclopedia, Vol. VI – Test Methods (Technomic Publishing Company, Inc., Lancaster, PA, USA, 1990) pp. 57–109.
[5] R. Prakash, Composites 11 (1980) 217.
[6] K.V. Steiner, in: Damage Detection in Composite Materials, Ed. J.E. Masters (ASTM, Philadelphia, PA, USA, 1992) ASTM-STP 1128, pp. 72–84.
[7] J.-P. Monchalin, J.-D. Aussel, P. Bouchard and R. Heon, in: Rev. Prog. Quantitative NDE, Eds. D.O. Thompson and D.E. Chimenti (Plenum, New York, 1988) Vol. 7B, pp. 1607–1614.
[8] H.M. Frost, in: Physical Acoustics, Eds. W.P. Mason and R.N. Thurston (Academic Press, New York, 1979) Vol. XIV, pp. 179–276.

[9] W. Sachse and N.N. Hsu, in: Physical Acoustics, Eds. W.P. Mason and R.N. Thurston (Academic Press, New York, 1979) Vol. XIV, pp. 277–406.

[10] C.A. Calder and W.W. Wilder, Mat. Eval. 38 (1980) 86.

[11] R.M. White, J. Appl. Phys. 34 (1963) 3559.

[12] D.A. Hutchins, in: Physical Acoustics, Eds. W.P. Mason and R.N. Thurston (Academic Press, New York, 1988) Vol. XVIII, pp. 21–123.

[13] C.B. Scruby and L.E. Drain, Laser Ultrasonics – Techniques and Applications (Adam Hilger, Bristol, 1990).

[14] W. Kuhl, G.R. Schodder and F.-K. Schröder, Acustica 4 (1954) 519.

[15] K. Suzuki, K. Higuchi and H. Tanigawa, IEEE Trans. Ultrason. Ferroelec. Freq. Contr. UFFC-36 (1989) 620.

[16] H. Carr and C. Wykes, Ultrasonics 31 (1993) 13.

[17] D.W. Schindel and D.A. Hutchins, IEEE Trans. Ultrason. Ferroelec. Freq. Contr. UFFC-42 (1995) 42.

[18] W.M.D. Wright, D.W. Schindel and D.A. Hutchins, J. Acoust. Soc. Am. 95 (1994) 2567.

[19] J. Hietanen, P. Mattila, J. Stor-Pellinen, F. Tsuziki, H. Väätäjä, K. Sasaki and M. Lukkala, Meas. Sci. Techn. 4 (1993) 1138.

[20] H. Carr, W.S.H. Munro, M. Rafiq and C. Wykes, Nondest. Test. Eval. 10 (1992) 3.

[21] M. Platte, Ferroelectrics 75 (1987) 327.

[22] H. Ohigashi, K. Koga, M. Suzuki and T. Nakanishi, Ferroelectrics 60 (1984) 263.

[23] L.C. Lynnworth, IEEE Trans. Sonics Ultrason. SU-13 (1965) 37.

[24] T.R. Gururaja, W.A. Schulze, L.E. Cross, R.E. Newnham, B.A. Auld and Y.J. Wang, IEEE Trans. Sonics. Ultrason. SU-32 (1985) 481.

[25] T.R. Gururaja, W.A. Schulze, L.E. Cross and R.E. Newnham, IEEE Trans. Sonics Ultrason. SU-32 (1985) 499.

[26] G. Hayward and J.A. Hossack, J. Acoust. Soc. Am. 88 (1990) 599.

[27] J.A. Hossack and G. Hayward, IEEE Trans. Ultrason. Ferroelec. Freq. Contr. UFFC-38 (1991) 618.

[28] D.A. Hutchins, W.M.D. Wright, G. Hayward and A. Gachagan, IEEE Trans. Ultrason. Ferroelec. Freq. Contr. UFFC-41 (1994) 796.

[29] G. Hayward and A. Gachagan, An evaluation of 1–3 connectivity composite transducers for air-coupled ultrasonic applications, submitted for publication to J. Acoust. Soc. Am.

[30] G. Hayward and J. Bennett, Assessing the influence of pillar aspect ratio on the behaviour of 1–3 connectivity composite transducers, submitted for publication to J. Acoust. Soc. Am.

[31] I.A. Viktorov, Rayleigh and Lamb Waves: Physical Theory and Applications (Plenum, New York, 1967).

[32] A.C. Kak and M. Slaney, Principles of Computerized Tomographic Imaging (IEEE Press, New York, 1988).

[33] D.A. Hutchins, D.P. Jansen and C. Edwards, Ultrasonics 31 (1993) 97.

[34] D.P. Jansen, D.A. Hutchins and J.T. Mottram, Ultrasonics 32 (1994) 83.